Soft Matter

PAPER

View Article Online
View Journal



Cite this: DOI: 10.1039/d5sm00572h

# Emergence and evolution of a particulate network during gelation and coarsening of attractive colloids

Paniz Haghighi,[a] Mohammad Nabizadeh[a] and Safa Jamali *[ab]

The process of gelation in attractive colloids involves formation of an interconnected and percolated network, followed by its coarsening and maturation. In this study, we analyze the formation and evolution of this particulate network and introduce deterministic quantitative measures to evaluate the key transition points. The rate of change in the number of colloidal clusters before and after percolation can be directly used to identify gelation as a continuous second order phase transition. Simultaneously the diameter of the particle network exhibits a distinguishable maxima, marking the precise moment of percolation transition. However, local measures of the structure such as coordination number do not reflect on the percolation. Alternatively, accumulative number of unique particle contacts can be used to indicate the long time coarsening of the particulate structure. Global structural measures such as Voronoi volume distribution and its changes over time can also be used to distinctly mark these two regimes. Finding a consistent behavior across varying attraction strength levels and volume fractions of colloids, we propose that percolation and coarsening of the particulate gels can be viewed as two distinct transitions with clearly distinguishable structural demarcations.

Received 2nd June 2025,
Accepted 1st September 2025

DOI: 10.1039/d5sm00572h

rsc.li/soft-matter-journal



## Introduction

Colloidal gels, a class of soft glassy materials, are ubiquitous in natural and industrial settings alike with applications in biotechnology, pharmaceuticals, cosmetics, and food technology.[1–10] In its general form, gelation of colloidal particles involves a transition from a liquid-like dispersion state to a soft solid-like percolated state. Nonetheless, this also means that a gel may be defined by either mechanical (liquid *vs.* solid) or structural (dispersed *vs.* percolated) criteria, depending on whether the emphasis is placed on the material's rheological behavior or its network connectivity. From a mechanical standpoint, the sol–gel transition corresponds to the divergence of the fluid's viscosity and/or the emergence of a measurable elastic modulus larger than the fluid's viscous response.[11–15] This clear macroscopic demarcation of gelation is commonly referred to as Winter–Chambon criterion.[11] However, in the case of polymer–colloid mixtures and weak depletion interactions, the rheological characterization of the resulting gel structure is known to be extremely challenging due to the very weak elastic modulus of the overall structure and its corresponding signal.[16–20]

From a purely structural viewpoint, the gelation transition is characterized by a dramatic slowdown in particle dynamics and the formation of a space-spanning particulate network.[12,21–25] The particulate network can form through a second-order phase transition,[26] in which particle-level bonds grow into clusters[12,27,28] and eventually result in percolation of the particulate structure spanning the entire system,[29–31] followed by long-term structure coarsening of the structure.[21,32] Other studies have considered gelation an arrested phase instability, in which the system undergoes spontaneous phase separation, forming regions rich and poor in colloids. This progression is stopped by attractive glass transition occurring in the colloid-rich region.[33] In thermo-reversible adhesive hard-sphere systems, gelation starts with a homogeneous percolation process[34,35] in which clusters driven by attractive forces span the entire system and mark the onset of gelation. This is supported by the observation that the experimentally determined gelation boundary closely aligns with the theoretically predicted dynamic percolation line.[36]

What is clear is that the macroscopic mechanics of gels are directly governed by their particulate network structures. From a mesoscopic perspective, recent developments suggest that the elasticity of the gel structure originates from the jamming transition of clusters.[37] This transition can be viewed as the formation of a glassy mesostructure of clusters[38] or space-filling soft particle glasses in a jammed structure.[28] The latter is consistent with descriptions of the hierarchical and multi-scale nature of the particulate network that controls the gel's

[a] Department of Mechanical and Industrial Engineering, Northeastern University, Boston, MA 02115, USA. E-mail: s.jamali@northeastern.edu
[b] Department of Chemical Engineering, Northeastern University, Boston, MA 02115, USA

mechanics as well.[12,39] Due to this close structure–mechanics coupling, understanding the evolution of the structure during and demarcating different stages of gelation can inform the targeted design of gels with desirable properties. In this work, we adopt a purely "*structural*" gel definition in which a gel is defined as any particulate network that spans the system size. Based on this definition, we do not measure/consider a mechanical gel definition, acknowledging that rheological/mechanical gel features may or may not strictly coincide with the structural transitions.

In addition to the main characteristics that define a gel, the intricate details of gelation kinetics, particularly closer to the sol–gel phase boundary, are also important. What is known is that colloidal gelation itself can follow different kinetics depending on the nature of the interaction between the particles, as well as state variables. In depletion gels, spinodal decomposition, depending on the state variables, including the volume fraction of the particles, as well as the range and strength of interactions between the particles,[22,24,33] primarily controls how and if a gel is formed. The structure and rate of spanning of the particle network are also influenced by different factors. It is well understood that gelation occurs through different mechanisms depending on the volume fraction of colloids. For intermediate volume fractions, gelation is initiated by the growth and subsequent percolation of fractal clusters. Conversely, for dense/crowded systems at higher volume fractions, gelation is generally induced by arrested phase separation marked by the formation of robust correlations between clusters.[40] The complexity of gelation is further affected by the strength of attraction between the particles. The attraction strengths affect the rate at which particles intermittently bond with and detach from their neighbors, which consequently affects the percolation of the space-spanning network. While very high attraction strengths can drive the system out of equilibrium, very weak attractions often lead to phase separation due to depletion interactions, resulting in the coexistence of liquid and crystal phases.[35,41]

Here, and building upon the non-equilibrium continuous phase transition view of the colloidal gelation, we present a comprehensive set of computational studies spanning a wide range of volume fractions and strengths of short-range attractions with the goal of characterizing the network formation and evolution during this transition. Our goal is to introduce quantifying measurements that successfully pinpoint the percolation point of the largest cluster and consequently the sol–gel transition point, as well as the coarsening of the structure after percolation. To predict the initial critical point in the structure transition, we utilize the percolation theory and the non-equilibrium continuous phase transition, which involves predicting the existence of a critical point and a power-law cluster-size distribution to define the sol–gel phase transition point. These are accompanied by power-law scaling consistent with the percolation theory as well as experimental observations of Zaccone *et al.*[37] Once this transition is clearly identified and the kinetics are established, we identify different measures of the colloidal particles' dynamics as well as the particulate network that marks this transition. At the last stage of the structure transition process, we study the coarsening of this network and discuss metrics that clearly identify the coarsening transition as a distinct phase. Ultimately, our study suggests that percolation and coarsening can be clearly distinguished by two quantifying measurements, providing a novel understanding of structural evolutions and different stages of gelation.

## Methods

To correctly model the interactions between particles while considering the essential hydrodynamics of the system with large numbers of particles, we use a dissipative particle dynamics (DPD) approach.[25] DPD is a mesoscale simulation technique based on molecular dynamics which was initially introduced by Hoogerbrugge and Koelman for the simulation of colloidal suspensions.[42] DPD considered hydrodynamic interactions, which is crucial for colloidal gels where fluid flow affects particle motion and aggregation.[25,28,43–46] The equation of motion of a DPD particle is written as:

$$F_i = m_i \frac{\mathrm{d}v_i}{\mathrm{d}t} = \Sigma\left(F_{ij}^{\mathrm{C}} + F_{ij}^{\mathrm{D}} + F_{ij}^{\mathrm{R}} + F_{ij}^{\mathrm{H}} + F_{ij}^{\mathrm{M}}\right) \quad (1)$$

The solvent particles interact only through $F_{ij}^{\mathrm{C}}$, $F_{ij}^{\mathrm{D}}$, and $F_{ij}^{\mathrm{R}}$ with other solvent and colloidal particles, representing the pairwise conservative, dissipative and random forces respectively:

$$F_{ij}^{\mathrm{R}} = \sigma_{ij} w_{ij}(r_{ij}) \Theta_{ij} \Delta t^{-1/2} e_{ij} \quad (2)$$

$$F_{ij}^{\mathrm{D}} = \gamma_{ij}[w_{ij}(r_{ij})]^2 (v_{ij} \cdot e_{ij}) e_{ij} \quad (3)$$

$$F_{ij}^{\mathrm{C}} = a_{ij} w_{ij}(r_{ij}) e_{ij} \quad (4)$$

Random force, eqn (2), is the source of thermal energy and Brownian motion in the system based on a random function of zero mean and unity variance, $\Theta_{ij}$, and strength of $\sigma_{ij}$. This thermal noise is then dissipated by the viscous resistance of the fluid, which are denoted as the dissipative forces eqn (3), that act against the relative motion of particles $v_{ij} = v_i - v_j$, with a magnitude of $\gamma_{ij}$. The simulation time step is denoted by $\Delta t$, and the unit interparticle distance vector is $e_{ij}$. In this formalism, $\gamma_{ij}$ and $\sigma_{ij}$ are coupled [through the fluctuation–dissipation theorem], defining the dimensionless temperature of the system as $\sigma_{ij} = \sqrt{2\gamma_{ij} k_{\mathrm{B}} T}$. The conservative forces with a magnitude parameter $a_{ij}$ that solely depend on the chemical identity of the particles give a DPD particle its pressure, eqn (4). All forces are controlled by a weight function that goes to zero as interparticle distance increases $w_{ij} = (1 - r_{ij}/r_{\mathrm{c}})$. Therefore, these forces become inactive when the interparticle distance exceeds a cutoff distance $r_{\mathrm{c}}$.

For colloid–colloid interactions, the conservative forces are absent, but dissipative and random forces act in the same manner as explained above. Since in DPD, when the distance between two colloids are smaller than a single solvent particle, hydrodynamics break down, an additional lubrication term, $F_{\mathrm{H}}$, is added to preserve the full hydrodynamics of the system:

$$F_{ij}^{\mathrm{H}} = \mu_{ij}^{\mathrm{H}} (v_{ij} \cdot e_{ij}) e_{ij} \quad (5)$$

 

In eqn (5), the lubrication force is calculated from the pair drag term $\mu_{ij} = 3\pi\eta_0 a^2/2h_{ij}$ where $a$ is the radius of the colloids, $h_{ij}$ is the surface–surface distance between two colloidal particles, and $\eta_0$ is the viscosity of the suspending fluid. The short-range attraction of the colloids is simulated by Morse potential, $F_M$:

$$U_{\text{Morse}} = U_0(2e^{-\kappa h_{ij}} - e^{-2\kappa h_{ij}}) \quad (6)$$

In eqn (6), $U_0$ determines the strength of attraction and $\kappa$ sets the range of attraction.

In our simulations, all quantities are reported in reduced DPD units, meaning that the fundamental physical parameters are nondimensionalized. The particle radius a is set to unity, and the dimensionless temperature of $k_BT = 0.1$, where $k_B$ is the Boltzmann constant. The mass of solvent particles is set to unity and the mass of colloidal particles is calculated as $m_c = 4\pi\rho a^3/3$, where $\rho$ is the number density. To match the system's density, The colloidal particles are simulated with a number density of $\rho = 3$. A number density ($\rho$) of 3 is a common choice in DPD simulations, largely due to the Groot–Warren method,[47] which connects DPD parameters to real-world properties. This value provides a stable balance between momentum transfer and thermal noise, and has become a widely accepted convention in the field.

To implement a short-ranged, weak attraction in the Morse potential, the range parameter $\kappa$ is set to 30, which corresponds to an interaction range of approximately $0.1a$. In other words, we want the attractive force between particles to become negligible beyond a separation of $h_{ij} = 0.1a$. This choice of $\kappa$ ensures that the exponential terms in eqn (6) decay rapidly, reducing the potential to about 4 percent of its original strength at that distance. Next, to nondimensionalize time, we use the single-particle diffusion time $\tau_d$ calculated from our simulation. We estimated $\tau_d$ by simulating a highly diluted system, where inter-particle interactions are negligible. The diffusion time $\tau_d$ is then defined as the time it takes for a particle to, on average, displace a distance equal to its own diameter, *i.e.*, MSD = $(2a)^2$. Once colloidal gels are prepared, a network analysis is performed on the particles. The connectivity of a pair of colloidal particles is defined as the separation distance at which the pairwise potential reaches zero energy.[48] For our systems, as previously discussed, this distance corresponds to $h_{ij} = 0.1a$. We have performed sensitivity tests (discussed in SI) and found that, while the exact percolation time shifts slightly with different thresholds, the overall qualitative behavior of percolation and structure evolution remains robust.

In this work, we analyzed the network formed by the particles in gels with volume fractions ranging from $\phi = 0.1$ to $\phi = 0.4$ and attraction strengths ranging from $U_0 = 6k_BT$ to $U_0 = 22k_BT$. The simulation box has a size of 60 times the colloidal particle radius ($a = 1$) in all directions. Hence, the number of particles in each gel varies with the volume fractions. For instance, at $\phi = 0.2$, the gel contains 10 313 particles, while at $\phi = 0.4$, the gel contains 20 626 particles. These system sizes are consistent with previous studies on colloidal gels and percolation. For instance, Del Gado and Kob used 8000 particles, and Li *et al.* used systems with 10 000 particles, both capturing percolation behavior reliably.[49,50] This suggests that our system size is appropriate for observing the same phenomena. To assess finite-size effects, we also conducted additional tests with smaller simulation boxes. As discussed in the SI, we find that the main structural and dynamic behaviors remain consistent provided that the simulation box is sufficiently large to avoid effects from periodic boundaries or wall effects.

Simulations were run for a total duration of $\tau_{max} = 62\tau_d$, with observables (*e.g.*, MSD, $Z$, $Z_{cu}$, kurtosis) evaluated at intervals of 10% of the diffusion time throughout the trajectory, which provides about ten frames for a particle to diffuse a distance equal to its diameter, giving us sufficient detail to track changes in particle motion and network evolution. The analysis spans the full time window, from initial cluster formation to late-stage coarsening, allowing us to capture percolation and coarsening behavior.

We compute several key measures of the structure as well as the particle dynamics in order to fully characterize particle assemblies. Mean squared displacement (MSD) is an ensemble averaged measure of the displacement for the particles with respect to a reference time, $t_0$, and a lag time, $t$:

$$\text{MSD}(t) = \langle |r_i(t_0 + t) - r_i(t_0)|^2 \rangle \quad (7)$$

On any snapshot of the particulate structure, the Voronoi volume for each particle and hence the overall distribution reflect the available hydrodynamic volume available to colloids. From the distribution histograms, we measure and track the kurtosis of the Voronoi volumes as the fourth standardized moment of the distributions:

$$\text{Kurt}(V_i) = E[(V_i - \mu/\sigma)^4] \quad (8)$$

where $V_i$ is the Voronoi volume, $\mu$ and $\sigma$ are its mean and standard deviation. and $E$ denotes the expected value.

# Results

### System design

In our system, we follow the formation and growth of aggregated particles, referred to as particle clusters. Particles are considered neighbors and part of the same cluster if the surface–surface separation distance between them is less than the sum of their radii and the range in which the attractive interactions are still significant (details provided in the Methods section). The simulations begin with fully dispersed and randomized positioned particles. Clusters grow as more particles progressively bond with one another and form a space-spanning network, after which the structure transition continues until the end of the coarsening. In this work, we study the transitions during which the particulate network spans the sample size, referred to here as the percolation transition and also the onset of gelation. This is because, our gels are defined purely from a structural point of view, and irrespective of their mechanical/rheological features. To do this, we define a particle cluster strictly as a single connected component made out of the bonded particles. Based on this definition, all clusters at time $t = 0$ are of size 1 [particle], growing over time, and in most

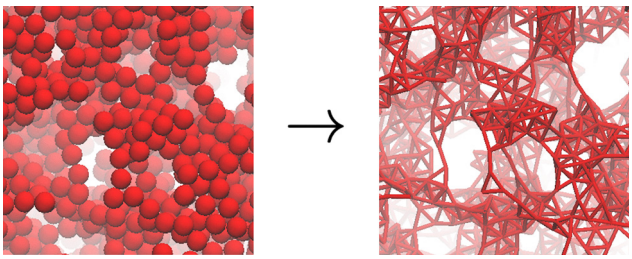

Fig. 1 Schematic view of the particles' and bonds' representation within each cluster or connected component, to be used for the purpose of network quantification.

cases grow to be of size equal to the number of particles. This definition directly reflects the most simply connected network that links an assembly of particles, without introducing additional structural constraints. Other clustering approaches in the literature target different physical attributes. For example, Gaussian Mixture Models (GMM), as used in our previous work[28] and in other studies,[51] aim to identify distinct substructures within the network based on statistical similarity rather than global connectivity. Similarly, the l-balanced method[38] captures the topology of rigid, load-bearing units within the gel, independent of precise spatial configurations. Graph-theoretic approaches based on isostaticity principles[52] identify rigid clusters by requiring that the particle contact number meets or exceeds the isostatic threshold, making them useful for studying bond breakage and rigidity transitions rather than percolation as defined here. In contrast, our connected-component criterion is designed specifically to determine simplest connected network. Therefore, For the remainder of this work, all results are measured from the analysis of the bonded structures, which are directly calculated from the positions of the particles (Fig. 1). In these analyses, a list of nodes and edges connecting those nodes, where particles are represented as nodes and particle–particle bonds as edges, is used, and the actual coordinates or any other particle-specific information is not carried over. Here, the same network analyses as in the work by Nabizadeh *et al.*[28] are employed to examine the characteristics of clusters and inter-particle interactions during the gelation process. All codes and algorithms can be directly accessed through our **https://rheoinformatic.com/website** and **https://github.com/procfGitHub** repository.

### Percolation transition

Fig. 2, from left to right, shows snapshots of our system of volume fraction $\phi = 0.2$ and attraction strength of $U_0 = 20k_BT$, with approximately 10 000 colloidal particles during the gelation process. The top row shows the particles, and the bottom row shows particle–particle bonds at the same snapshot, color-coded with respect to the number of particles in each cluster (lighter colors representing smaller clusters). As clearly indicated in this figure, at any point during the structure transition, many clusters/connected components exist within the system, starting with $N_{cluster} = N_{particle}$ and, in most cases, ending with $N_{cluster} = 1$. However, it is reasonably safe to assume that the properties of the overall system are controlled by the largest connected component or cluster within its structure. Thus, in order to identify the exact time of percolation transition during gelation, we follow the largest existing cluster at each step of the structure transition. While this approach provides a rigorous and clearly defined quantitative measure of structure evolution, it also poses a challenge, as the transition near the point of percolation can occur rapidly. To demonstrate the challenges in exactly identifying the percolation transition,

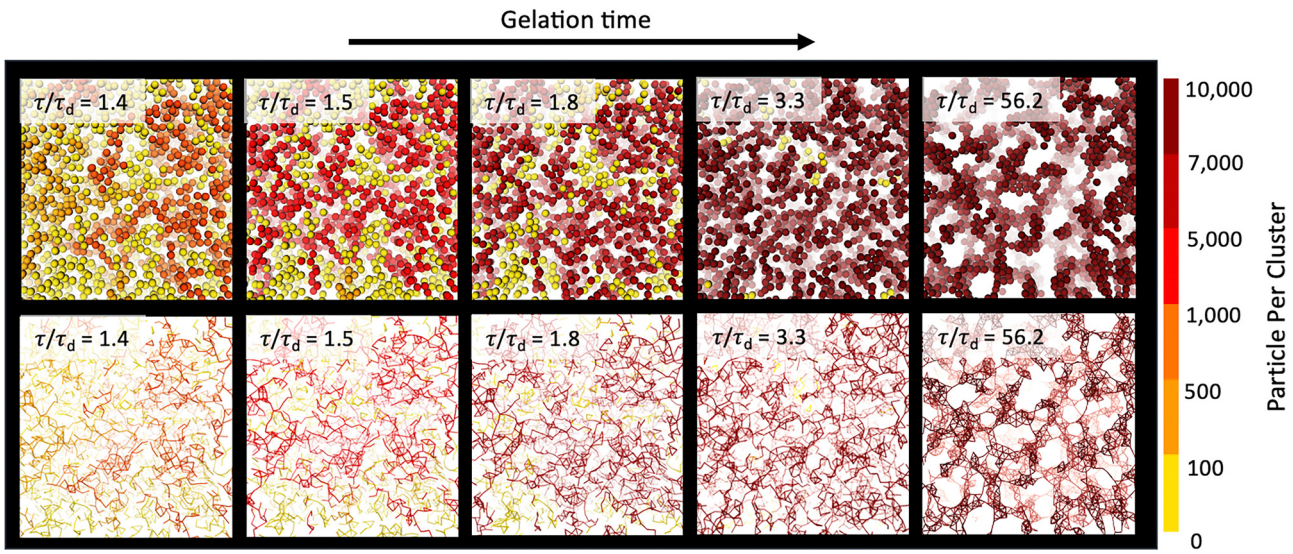


Fig. 2 Snapshots of a colloidal system with a volume fraction of $\phi = 0.20$ and an attraction strength of $U_0 = 20k_BT$ undergoing gelation at dimensionless times ($\tau/\tau_d$) 1.4, 1.5, 1.8, 3.3, 56.2 from left to right, where $\tau_d$ is the diffusion time. (Top row): Colloidal assemblies, and (bottom row): their resulting bonded structures over time. All colloids and their bonds are color-coded with respect to the number of particles within the clusters, provided in the scale bar. The process begins with the absence of large clusters in the initial stage and progresses to the largest cluster spanning the entire system, and ends with the coarsening of the particulate network.

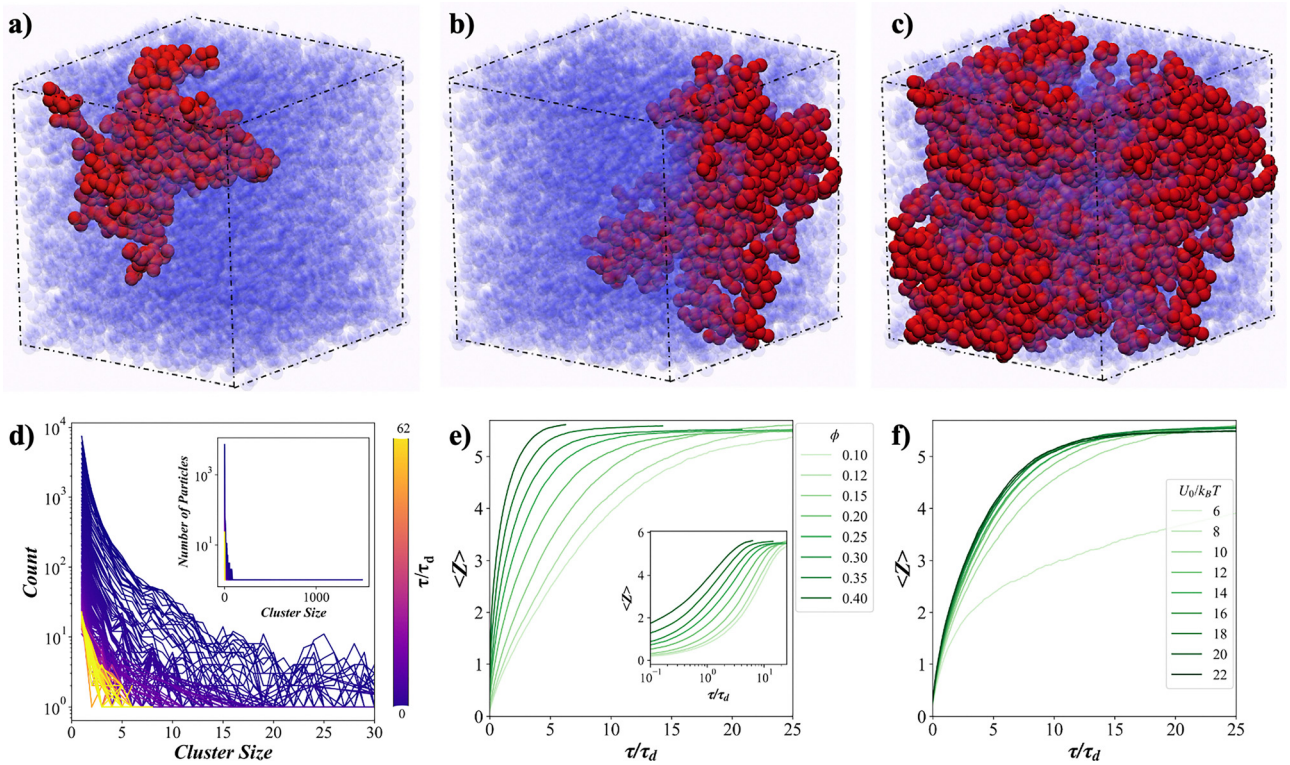


Fig. 3 (a)–(c) Three different snapshots of the largest connected component within the system during gelation at times ($\tau/\tau_d$) 1.3, 1.4, and 1.5, respectively, for a system with $\phi$ = 0.2 and an attraction strength of $U_0 = 20k_BT$. (d) Cluster size distribution during gelation, excluding the largest cluster for the same system. The cluster size represents the number of colloidal particles within each individual cluster. Changes in the ensemble-averaged coordination number, $\langle Z \rangle$, during gelation for: (e) different volume fractions at an attraction strength of $U_0 = 20k_BT$, and (f) different attraction strengths at the volume fractions of $\phi$ = 0.2.

the largest clusters in the system with a volume fraction of 0.2 and an attraction strength of $U_0 = 20k_BT$ are shown in red at times 1.3$\tau$, 1.4$\tau$, and 1.5$\tau$ in Fig. 3(a)–(c), respectively. While in Fig. 3(a), the largest cluster does not percolate across the system size, in Fig. 3(b), it does reach the size of the system in one direction; however, since the cluster only spans the system size in one direction, it is not plausible to consider the overall structure percolated. In contrast, the largest cluster in Fig. 3(c) clearly spans the system size in all directions and thus can be considered a fully percolated structure. This is particularly noteworthy since the entire change in this transition occurs within a fraction of the diffusion time. The size distribution of the clusters, excluding the largest cluster, in Fig. 3(d) also shows that the size of the remaining clusters reduces rapidly. Hence, their contributions are negligible.

In colloidal gels, percolation has been linked to power law scaling of different measurables, including the elastic modulus, viscosity, correlation length, and the fraction of particles within the largest cluster.[11,26,40,53] However, these studies do not pinpoint the critical point of percolation. Instead, the critical point is generally approximated through interpolation techniques or by tracking the divergence patterns within the plots. Here, we introduce a precise measurement to accurately identify this transition point. The most common quantitative measure of the local microstructure for a colloidal assembly is the ensemble-averaged number of bonds that each particle makes, referred to as the coordination number. The average coordination number as a function of time is plotted for a wide range of particle volume fractions and at the attraction strength of $U_0 = 20k_BT$ in Fig. 3(e). Evidently, the average coordination number grows for all volume fractions studied and eventually reaches a plateau at values of $Z > 5$. Note that the highest volume fraction of particles studied here remains below the glassy regime. Thus, all the observed structures can be compared without considering the possibility of forming bulk glassy structures. On the other hand, the ensemble-averaged $Z$ as a function of time for different attraction strengths at a constant volume fraction of $\phi$ = 0.2, shown in Fig. 3(f), indicates that the number of bonded neighbors per particle is primarily controlled by the interaction potential. This is particularly evident at an attraction strength of $U_0 = 6k_BT$, where the final number of bonded neighbors is more affected by the attraction strength than by the volume fraction. It also explains the very small variation of the average $Z$ values for different volume fractions depicted in the inset of Fig. 3(e).

Next, we monitor the fraction of particles that belong to the largest cluster in the system over time for a single attraction strength of $U_0 = 20k_BT$, shown in Fig. 4(a). It is clear that in all studied volume fractions of $\phi > 0.12$, almost all particles eventually become part of the largest cluster within the system.

However, for $\phi \leq 0.10$, the largest cluster within the system remains smaller than half of the particle population, and the system never reaches a fully percolated state in all directions. For both average coordination number and fraction of particles within the largest cluster, the stronger attractions, as well as higher volume fractions of particles result in faster percolation kinetics (Fig. 4(b)). Nonetheless, the observed trends in the variation of $f$ over time clearly indicate a critical percolation time to exist.

Since both the coordination number and the fraction of particles within the largest cluster follow similar trends over time, and following the work of Rouwhorst *et al.*,[26] we next show the variations in the fraction of particles in the largest cluster as a function of $Z$, the coordination number, in Fig. 4(c) and (d). The results in Fig. 4(c) indicate that the number of colloids within the largest cluster shows a consistent behavior for different systems with a clear percolation transition that is only controlled by the overall volume fraction. For lower volume fractions, this transition occurs at higher coordination numbers, and for higher volume fractions, percolation happens at smaller coordination numbers. For lower volume fractions ($\phi \leq 0.10$), the system is more dilute, and percolation occurs at or after dynamic arrest.[54] Therefore, there's minimal distinction between the onset of percolation and the end of coarsening, as shown in Fig. 4(d). In contrast, at higher volume fractions ($\phi \geq 0.15$), the system is denser, exhibiting a distinct percolation transition. This observation aligns with findings that volume fractions between $\phi = 0.1$ and $\phi = 0.15$ represent a transitional regime between dilute and dense behaviors.[54] Hence, for $\phi \geq 0.15$, and when the system has distinct percolation and gelation points, determining the critical coordination number and the percolation point becomes challenging as the exact position of this transition can be elusive. Given these complexities, we focus on dense gels ($\phi \geq 0.15$) and find the critical coordination point for these systems.

Our approach to pinpoint the percolation transition lies within the measurement of the cluster diameter, $D$, during percolation. From a network perspective, the diameter is the longest of the shortest paths between any two nodes within its structure, providing a common measure of its size.[55] This concept is illustrated schematically in Fig. 4(e). To calculate this quantity, for each combination of two nodes (particles) within a cluster, the shortest path connecting those two nodes is determined. Doing this iteratively and for all possible combinations of any two nodes within a network, the longest of all shortest paths is then found and identified as the diameter of the network. For instance, for a linear chain of $N$ connected components, the diameter of the network will always be $N - 1$. Interestingly, for volume fractions corresponding to percolated structures, the diameter of the network exhibits a sharp maximum when plotted against time in Fig. 4(f). Even at the lowest volume fraction, the maximum network diameter exceeds the system's box size, which is 60 times the particle radius. This observation indicates that the largest connected component occupies a significant portion of the system at this time. The normalized network diameter (by the maximum diameter measured) is plotted as a function of coordination number in Fig. 5(a), alongside the fraction of particles within the largest cluster. Not only does the network diameter for all attraction strengths studied (shown using color increments) show a

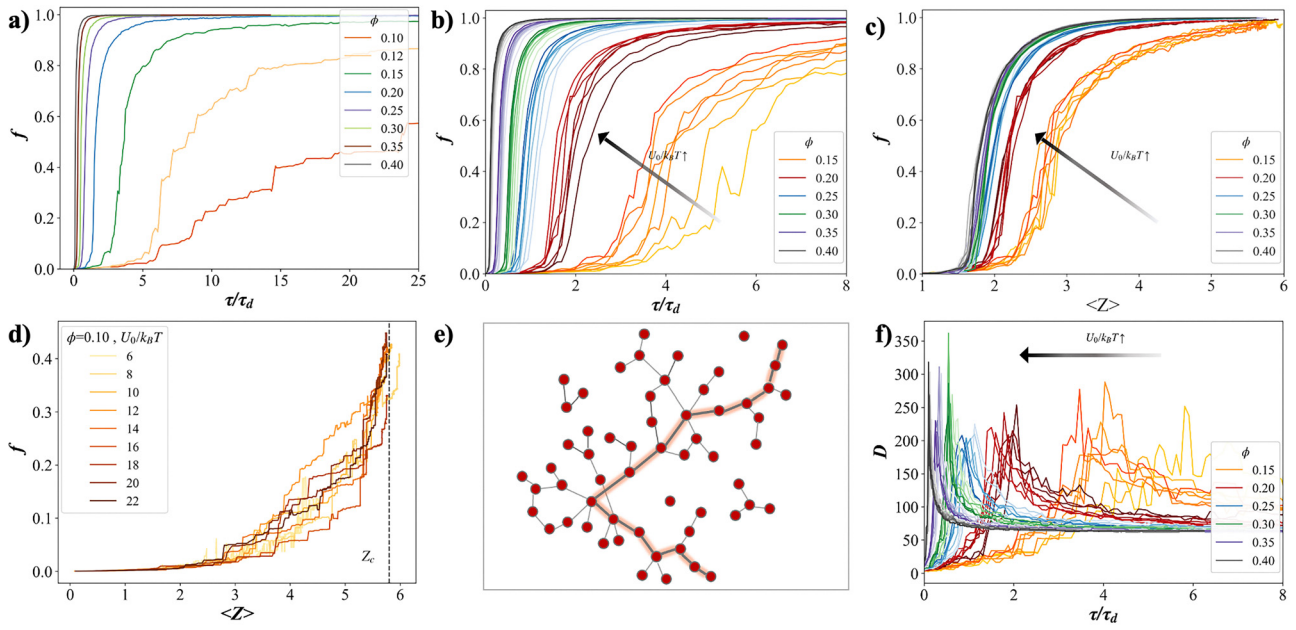


Fig. 4 Fraction of total particles in the largest cluster for: (a) all volume fractions and the attraction strength of $U_0 = 20k_BT$ *versus* gelation time; (b) and (c) volume fraction of $\phi \geq 0.15$ and all attraction strength, plotted *versus* gelation time and *versus* the ensemble-averaged coordination number, $\langle Z \rangle$, respectively; (d) volume fraction $\phi = 0.1$ and all attraction strength.(e) Schematic illustrating the diameter of a particle network, defined as the longest among all shortest paths between pairs of particles. The highlighted line marks the two particles connected by this path.(f) Network diameter *versus* gelation time for systems with $\phi \geq 0.15$.

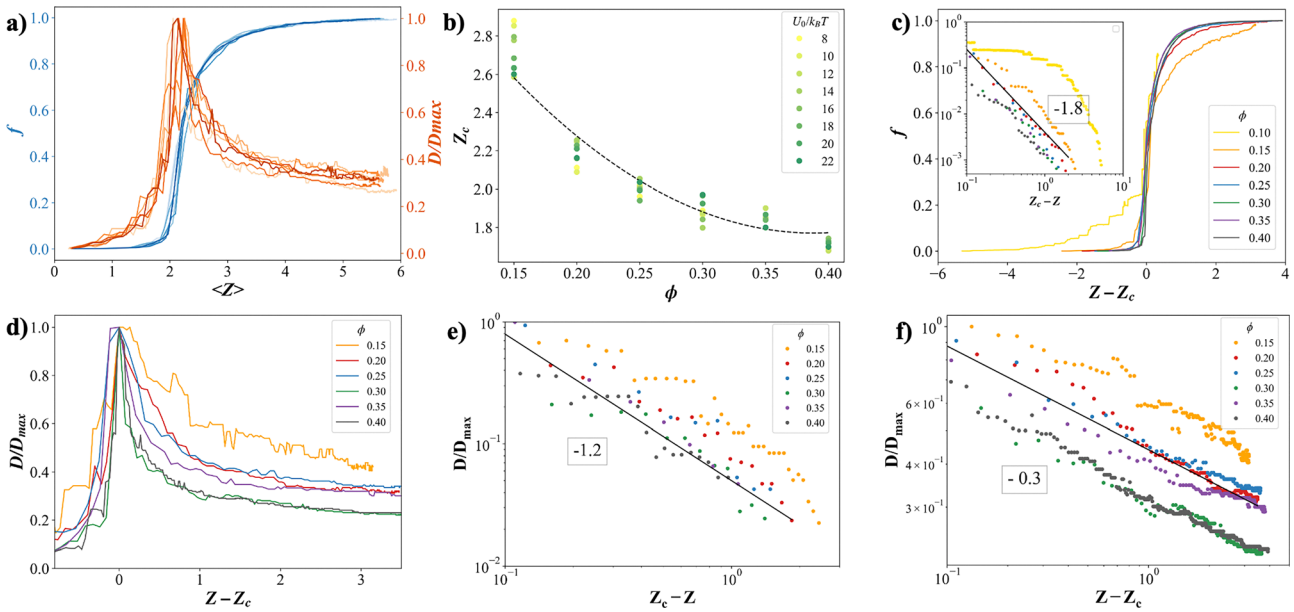


Fig. 5 (a) Normalized network diameter (by its maximum value) and the fraction of particles within the largest connected components *versus* the ensemble-averaged coordination number, $\langle Z \rangle$, for all attraction strengths at $\phi = 0.2$. (b) Critical coordination number, $Z_c$, for different attraction strengths and volume fractions. (c) Fraction of particles within the largest connected component, $f$, *versus* the re-scaled coordination number for all volume fractions at the attraction strength of $U_0 = 20k_BT$. The insert figure shows the same data in a power-law plot, characterized by an exponent of −1.8. (d)–(f) The diameter of the largest cluster as a function of the re-scaled coordination number, featuring an exponent of −1.2 before (e), and −0.3 after (f) the critical point for all volume fractions.

universal behavior, but their maxima also appear to exactly coincide with the percolation transition, regardless of the volume fraction (Fig. 5(a) is plotted for $\phi = 0.2$). From the position of $D_{max}$, we accurately identify the values of $Z_c$ for different values of $\phi$ and attraction strengths. Fig. 5(b) presents the critical coordination number $Z_c$, for $\phi \geq 0.15$ for all attraction strengths. the changes in the critical coordination number are mostly dependent on $\phi$, rather than the attraction strength, which is illustrated by a trend line.

Upon approaching the critical coordination number for percolation, $Z_c$, the fraction of particles within the largest cluster follows a power law equation of $[f_z = (Z_c - Z)^{\gamma}]$, with the exponent $[\gamma = -1.8]$ for all percolated systems, and completely deviates from this behavior for the systems that do not reach a percolated state (Fig. 5(c)). This exponential behavior is consistent with the ones from similar systems experimentally studied by Ruowhorst and coworkers,[26] and the exponents governing the divergence show consistency with the three-dimensional percolation theory and the exponents of the random percolation universality class.[33] As the system approaches this critical percolation point, the diameter of the network also follows a power law equation before $[D = (Z_c - Z)^{\mu}]$ and after $[D = (Z - Z_c)^{\nu}]$ the percolation, with exponents denoted as $[\mu = -1.2]$ and $[\nu = -0.3]$, shown in Fig. 5(d)–(f). The percolation transition time ($P_{c1}$), measured as the time at which the system reaches the $Z_c$, is plotted for different volume fractions and attraction strengths studied in Fig. 6. The overall percolation time gradually decreases as the strength of attraction is increased, indicating that the strongly attractive systems are faster to percolate. On the other hand, the

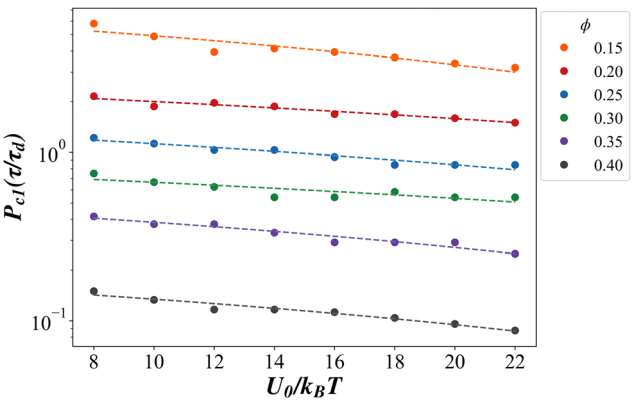


Fig. 6 The percolation time, $P_{c1}$, for different volume fractions and attraction strengths.

overall scale of this transition time is entirely controlled by the volume fraction of colloidal particles.

Given the consistency of the power law scaling across various systems studied, we assert that the critical point identified here is valid for both low and high volume fractions, as well as for relatively weak to very strong attractions. Furthermore, the power-law behavior of the cluster diameter can also be used directly as another parameter exhibiting a universal behavior at the percolation threshold.

### Structure coarsening

Thus far, our results have shown that the percolation transition can be directly measured using the size and number of clusters

within a system. Nonetheless, post-percolation, the system continues to evolve and undergo a coarsening process over time. In this stage, particles can further rearrange and result in denser domains with different characteristics which in turn also affects the overall mechanics of the gels. From a rheological perspective, a just-percolated network may not necessarily result in an elastic modulus larger than the viscous modulus. Therefore, it is plausible to assume that rheological identifications of gel point are more consistent with the coarsening stage rather than the percolation. However, this also depends on other parameters such as attraction strength and bending elasticity of the particle bonds. At the same time, microstructural measures of the system such as the number of connected components and the coordination number often reach a quasi-steady plateau during coarsening and may not reflect the continuous evolution of the structure.

Although the average number of neighbors around a particle remains largely constant during the coarsening step, it is well understood that the structure is not completely arrested, and local rearrangements continue to age the overall structure. Having access to all bonds that form and break over the entire time of structure evolution, we introduce an alternative measure of the microstructure: the average cumulative unique neighbors $Z_{cu}$ shown in Fig. 7(a). To calculate $Z_{cu}$, all inter-particle bonds throughout the simulation are tracked, and the number of unique neighbors that a single particle bonds with during the entire process is determined. For instance, as shown in Fig. 7(b), if particle A remains in contact with particles B, C, and D at time $t$, then $Z^{A}_{cu} = Z^{A} = 3$; but if after a time interval $\delta t$, the A–C bond is broken and instead a new bond of A–E is made, then $Z^{A}_{cu} = 4$ and $Z^{A} = 3$. Hence, the cumulative number of unique neighbors will be reflective of the structure evolution even if the average coordination number itself remains unchanged. The changes of $Z_{cu}$ over the entire evolution time in Fig. 7(a) indeed shows a very clear two step process. During initial times of gelation [and well past the percolation transition marked by the vertical dashed line in the figure], the number of unique neighbors explored by a single colloid at any time is virtually the same for all strengths of attraction, and is instead only controlled by the fraction of solid particles. This is somewhat expected as the probability of particles bonding with one another inversely correlates with the separation distance between them and hence directly with the volume fraction of particles (population dominated). On the other hand, once these local structures (clusters) are formed and particles are somewhat arrested in their respective cages, the probability of hopping out of their cage and making a new bond becomes entirely independent of the overall volume fraction and is instead controlled solely by the strength of attraction between the particles (attraction dominated). What is surprising is that the initial diffusive growth of $Z_{cu}$ with time continues well past the percolation transition and the overall arrest of the structure, suggesting that a second characteristic time [end of coarsening], $P_{c2}$, can be defined to distinguish between these two processes.

Our observations reveal a consistent trend in the initial section across all levels of attraction strength. Fig. 8(a)–(c) shows that for a given attraction strength and varying volume fractions, the slopes of the plots before and after the second critical point are identical, following the same overall trend. This demarcation of the second critical transition, $P_{c2}$, can also be defined as the transition from a population-dominated to an attraction-dominated regime. In Fig. 7(a), the two critical transition times (percolation and coarsening) are shown *via* vertical dashed lines. One should note that for stronger attractions, and some volume fractions, the two can be very close; however, in all of our studied systems, they can be measured at distinctly different times.

The list (and thus the number) of unique neighbors throughout the structure evolution is extremely challenging (if not impossible) to obtain experimentally. Thus, we next explore other tangible measures [from an experimental perspective] that can also be used to hint at this second coarsening transition. A common measure of the system's microstructure is Voronoi volume tessellation, which provides a measure of available volume to each particle within a given structure.[56]

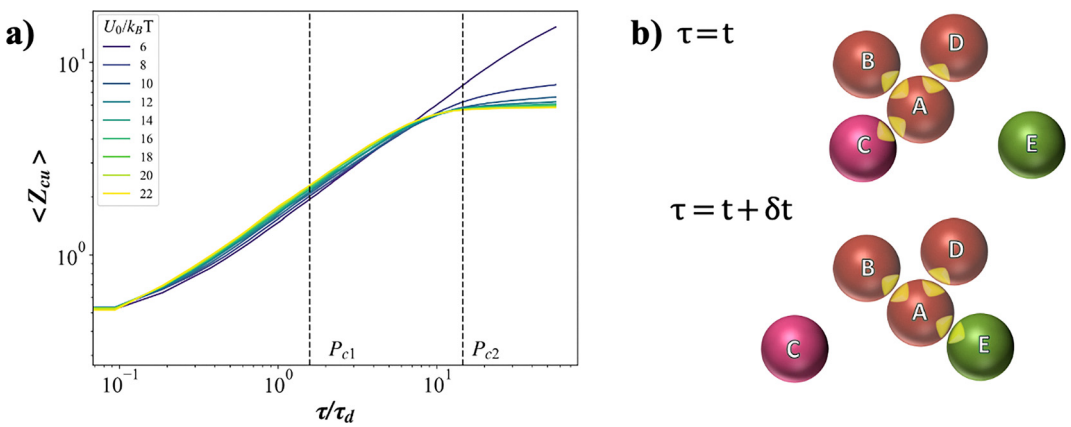


Fig. 7 (a) Cumulative unique neighbors, $Z_{cu}$, of particles during gelation for $\phi$ = 0.20 and different attraction strengths. Both transition points, $P_{c1}$ and $P_{c2}$, are marked using vertical lines. (b) Schematic view of changes in $Z_{cu}$, in upper image at time $t$, with $Z^{A}_{cu} = Z^{A} = 3$, and at time $t + \delta t$ with $Z^{A}_{cu} = 4$ and $Z^{A} = 3$.

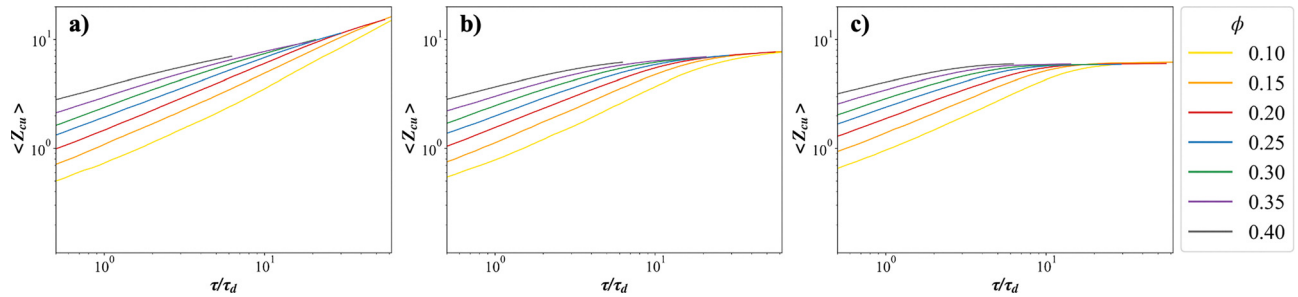


Fig. 8 Ensemble-averaged unique coordination number, $Z_{cu}$, *versus* gelation time (scaled by the particle diffusion time) for different volume fractions at the same attraction strength of: (a) $U_0 = 6k_BT$, (b) $U_0 = 8k_BT$, and (c) $U_0 = 20k_BT$.

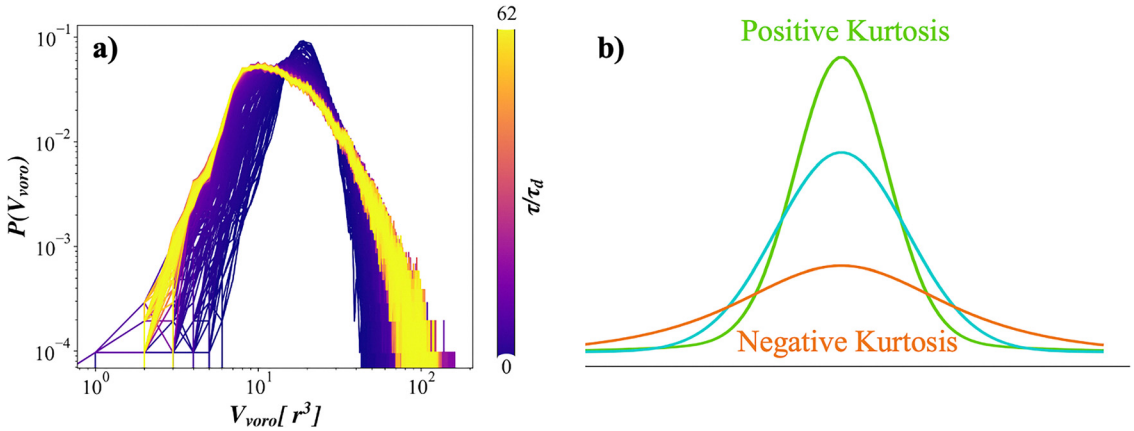


Fig. 9 (a) Voronoi volume distribution at different times during the gelation process of a system with $\phi = 0.2$ and $U_0 = 20k_BT$. (b) Schematic depiction of kurtosis, showing variations in data distribution at the peak and tails.

As such, a Voronoi volume distribution graph for a gel can be used as a proxy to structural evolution over time. Fig. 9(a) illustrates a typical Voronoi volume distribution for a system with a volume fraction of $\phi = 0.2$, and an attraction strength of $U_0 = 20k_BT$ at different steps of the gelation process. Since the overall volume (area under the curve) will remain constant for each system, *i.e.* constant volume of the simulation box or experimentally imaged window, and since the Voronoi volume distributions are non-trivial bell-shaped curves, a detailed exploration inherently involves quantifying the curves over time. In our study, we focus on the changes in kurtosis of the Voronoi volume distribution curves over time, corresponding to the distribution of data in the tails and peaks. A schematic view of changes in kurtosis is shown in Fig. 9(b). Typically, larger kurtosis values suggest magnified peaks with narrower distributions, while smaller values hint at broader distributions with fat tails.

Fig. 10(a) illustrates the changes in Voronoi volume distribution's kurtosis measures during the process of gelation for a system with a volume fraction of $\phi = 0.2$ and different attraction strengths, which reveal three clear regions for each attraction strength that coincide with the two critical transition points of the gelation process. The kurtosis first shows an initial plateau, followed by a clear increase before the coarsening transitions. A high value of kurtosis suggests that more particles are found with volumes available to them corresponding to the tails and the peak of the distribution, hinting at the formation of larger voids as well as densely packed structures. The changes in the kurtosis in Fig. 10(a) also exhibit a behavior reminiscent of the cumulative unique neighbors $Z_{cu}$. During the initial gelation stage, all systems with different strengths of attraction show a similar behavior that is: upon percolation the kurtosis begins to grow as the particle-rich and particle-depleted regions within the system's structure form and evolve, solely dominated by the diffusion of particles and rather independent of their interaction potential. However, once the overall coarsened structure is formed and the dynamics begin to slow down, curves can be differentiated based on the details of their interaction potential.

Mean squared displacement (MSD) is another quantitative measure of the dynamical arrest in colloidal gels which is used to evaluate the gelation of colloidal particles as it reflects the progressive slowing down of particle motion within the system. Gelation process usually begins with the diffusive motion of the particles followed by a transition to sub-diffusive behavior during gelation and arrest of the structure, which may or may not result in a second diffusive region reflective of the cage-hopping and re-entrant nature of the gels at very long times. Since the two measures introduced here, namely the kurtosis of the Voronoi volume distribution and the unique cumulative neighbors, $Z_{cu}$, provide a very distinguishable time for each of

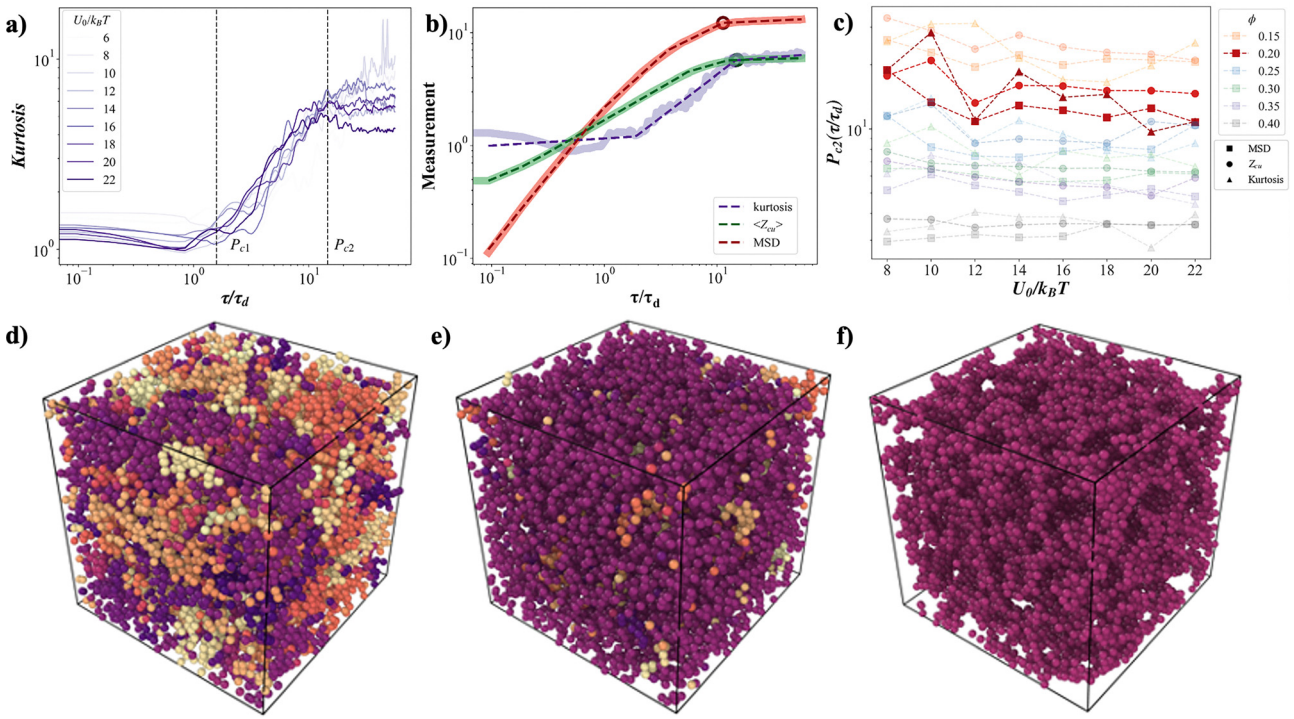


Fig. 10 (a) Kurtosis of the Voronoi volume distribution *versus* time for various attraction strengths for the system with $\phi$ = 0.2. (b) Comparison of the second transition point across different measurements: mean square displacement (MSD), kurtosis, and unique neighbors ($Z_{cu}$) for a system with volume fraction $\phi$ = 0.2 and attraction strength $U_0 = 20k_BT$. The plots are analyzed using linear regression, indicated by dashed lines. The point of slope change is marked as the second transition point. (c) The second critical point measured from $Z_{cu}$ (circles), MSD (squares), and kurtosis (triangles) for $\phi \geq 0.15$ and all attraction strengths. Snapshots of the system with $\phi$ = 0.2 and $U_0 = 20k_BT$: (d) before percolation, (e) at the percolation point, and (f) at the second transition point and end of coarsening. colors indicate particles belonging to the same cluster.

the percolation and coarsening transitions, we next compare those measures with the MSD of the systems. Fig. 10(b) shows the evolution of the three measurements during the gelation process for a representative system with a volume fraction of $\phi$ = 0.2 and an attraction strength of $U_0 = 20k_BT$. Using linear regression, we identified the point at which the mean squared displacement (MSD) plateaus, marking the onset of dynamical arrest. Similarly, we applied the same method to determine the points where the slope of the unique cumulative neighbors and kurtosis changes, representing the second transition point and the end of coarsening. These identified transition points allow us to compare the three measurements at the second transition point. Fig. 10(c) shows this comparison for $\phi \geq 0.15$ across all attraction strengths, with the values for $\phi$ = 0.2 highlighted in darker red for clearer comparison. Remarkably, not only do $Z_{cu}$ and MSD align in behavior, but kurtosis also shows similar pattern. This alignment is more evident when compared with the other volume fractions. For systems where dynamic arrest either has not occurred or is impeded due to very weak attraction strength, we observe that, in addition to MSD and $Z_{cu}$, kurtosis fails to plateau. Consequently, the system doesn't reach the second transition point, and there is no arrest in the system. Conversely, in systems with higher attraction, kurtosis distinctly exhibits a plateau and follows the same trajectory as MSD and $Z_{cu}$. Notably, the moment at which kurtosis converges with the two and plateaus almost aligns with the same moment as $Z_{cu}$ entering its attraction-dominated stage and the MSD enters sub-diffusive region. Our assertion is that changes in the kurtosis of the Voronoi volume distribution during the gelation process along with the cumulative unique neighbors $Z_{cu}$ can be used to mark the second transition, a.k.a coarsening. Finally, in Fig. 10(d)–(f), a schematic representation of the system's structure is provided to clarify the comparison of the structural differences at different stages, where the colors indicate particles belonging to the same cluster. The schematic demonstrates that, although a space-spanning network forms at the percolation point, the system continues to coarsen until it reaches the second transition point. At this stage, the particles become more aggregated and compact. Beyond this point, the system undergoes further aging, eventually reaching the gel point, signaling the completion of the gelation process.

## Discussion and conclusions

In this work, we study the process of colloidal gelation in which a particle network forms as a result of attraction between individual colloids. Identifying and characterizing the critical transitions that mark the construction and evolution of the underlying network of connections [between individual components] holds the key to describing the mechanics of colloidal gels (as typical soft glassy materials). Hence, using concepts

from percolation theory and non-equilibrium continuous phase transition, we quantify these transitions as gels with different state variables are formed. One key observation is that the first critical point, $P_{c1}$, corresponding to the sol–gel transition, is marked by a clear maximum in the diameter of the largest connected colloidal cluster. This is the point where the largest cluster first percolates the entire system. We also found that both the fraction of particles and the diameter of the largest cluster exhibit a power-law relationship with the coordination number. Remarkably, the scaling exponents are consistent across different percolated structures with varying volume fractions and attraction strengths. Different structural and dynamical characteristics also suggest that the first critical point lies within a population-controlled regime, where the system's behavior is predominantly influenced by the total volume fraction of particles and, hence, by the diffusion of individual particles. At this point, despite witnessing growth in the largest cluster, gelation remains continuous as the bonding between particles remains weak. This population-controlled regime is followed by an attraction-controlled one that is marked by the sudden change in cumulative unique neighbors and kurtosis of the Voronoi volume distribution. This abrupt alteration signifies the occurrence of the second critical transition, $P_{c2}$, indicating the coarsening stage of gelation. The transition to this stage is a function of the strength of attraction between the particles, with higher attractions causing an earlier transition.

While the precise $P_{c2}$ values from the three measurements differ slightly, they are in close agreement (Fig. 10(c)). More importantly, the $P_{c2}$ obtained from $Z_{cu}$ and the kurtosis of the Voronoi volume distribution, both indicating structural arrest, closely matches the $P_{c2}$ from the MSD, which indicates dynamical arrest. Together, these results mark the arrested dynamics of the network, and the end of coarsening. While this behavior shares some similarity with glass transition, where particles are trapped in cages and escape *via* hopping, there are key differences.[57,58] In glassy systems at higher volume fractions, cage hopping is very different from local energy explorations of a particle within a gel cluster. In recent years, a picture of gel mechanics has emerged, suggesting that clusters of particles are in glassy regime.[28,38] However, at the particle-level, dynamics clearly deviate from ones in glassy state. After $P_{c2}$, and depending on the strength of attraction, particles can still explore new neighbors, though at a different pace. But these are not due to cage hopping, as particles do not lose their entire neighboring colloids and remain bonded within their respective clusters.

From a mechanistic perspective, gels are formed when rigidity, and not connectivity, is percolated. This is elegantly demonstrated in work of Zhang *et al.*,[59] where rigidity percolation is defined as the emergence of a system-spanning rigid network, with its occurrence determined by both volume fraction and attraction strength. Of course, for the rigidity to percolate, connectivity should be already percolated as well. Thus, comparing the structural percolation, and mechanical percolation, the former occurs first and is a prerequisite. Future work on testing the concept of rigidity percolation in 3D networks and on our studied systems can be informative in better understanding the structural signatures of rigidity percolation as well.

Our results clearly indicate that the dynamics of colloidal gelation can be considered to be a two-step process: the first step being a second-order non-equilibrium continuous phase transition to a percolated state, followed by a second stage that ultimately forms the final morphology of the colloidal gel, referred to as coarsening. These two steps are associated with clear quantitative measures of the structure and are also representative of two distinct mechanics. Earlier work of Rouwhorst *et al.*[26] suggested that for intermediate volume fractions of particles, this second-order non-equilibrium phase transition can be viewed analogously to classical percolation in 3D. Our findings are fully consistent with their findings, and are universally observed over a wide range of volume fractions and attraction strengths. This suggests that building a universal understanding of the fluid-to-solid transition in disordered conditions may be possible through the characterization of the collective/network kinetics during this transition.

## Conflicts of interest

There are no conflicts to declare.

## Data availability

All data, codes, and algorithms can be directly accessed through **https://rheoinformatic.com/** and **https://github.com/procf**.

The supplementary information provides sensitivity analyses of connectivity distance and simulation box size, to ensure the robustness of our measurements. See DOI: **https://doi.org/10.1039/d5sm00572h**.

## Acknowledgements

Authors would like to acknowledge support from the National Science Foundation DMREF program through Award 2118962.

## References

1 S. C. Dennis, M. S. Detamore, S. L. Kieweg and C. J. Berkland, Mapping glycosaminoglycan-hydroxyapatite colloidal gels as potential tissue defect fillers, *Langmuir*, 2014, **30**(12), 3528–3537.
2 T. Ferreira-Gonçalves, C. Constantin, M. Neagu, C. P. Reis, F. Sabri and R. Simón-Vázquez, Safety and efficacy assessment of aerogels for biomedical applications, *Biomed. Pharmacother.*, 2021, **144**, 112356.
3 A. Mirtaghavi, J. Luo and R. Muthuraj, Recent advances in porous 3d cellulose aerogels for tissue engineering applications: a review, *J. Compos. Sci.*, 2020, **4**(4), 152.

4 M. Carrancá Palomo, V. Martn Prieto and P. Kirilov, Colloidal dispersions of gelled lipid nanoparticles (Gln): concept and potential applications, *Gels*, 2017, **3**(3), 33.
5 Z. Wei, J. H. Yang, J. Zhou, F. Xu, M. Zrnyi and P. H. Dussault, *et al.*, Self-healing gels based on constitutional dynamic chemistry and their potential applications, *Chem. Soc. Rev.*, 2014, **43**(23), 8114–8131.
6 L. Gonçalves, P. Lavrador, A. J. Amaral, L. P. Ferreira, V. M. Gaspar and J. F. Mano, Double-Interlinked Colloidal Gels for Programable Fabrication of Supraparticle Architectures, *Adv. Funct. Mater.*, 2023, **33**(45), 2304628.
7 L. B. Cappeletti, E. Moncada, J. Poisson, I. S. Butler and J. H. Z. D. Santos, Determination of the network structure of sensor materials prepared by three different sol–gel routes using Fourier transform infrared spectroscopy (FT-IR), *Appl. Spectrosc.*, 2013, **67**(4), 441–447.
8 R. Martinez, C. Rosado, M. V. R. Velasco, S. C. D. S. Lannes and A. R. Baby, Main features and applications of organogels in cosmetics, *Int. J. Cosmet. Sci.*, 2019, **41**(2), 109–117.
9 A. Ashfaq, K. Jahan, R. U. Islam and K. Younis, Protein-based functional colloids and their potential applications in food: a review, *LWT*, 2022, **154**, 112667.
10 R. Mezzenga and P. Fischer, The self-assembly, aggregation and phase transitions of food protein systems in one, two and three dimensions, *Rep. Prog. Phys.*, 2013, **76**(4), 046601.
11 H. H. Winter and F. Chambon, Analysis of linear viscoelasticity of a crosslinking polymer at the gel point, *J. Rheol.*, 1986, **30**(2), 367–382.
12 M. Bantawa, B. Keshavarz, M. Geri, M. Bouzid, T. Divoux and G. H. McKinley, *et al.*, The hidden hierarchical nature of soft particulate gels, *Nat. Phys.*, 2023, **19**(8), 1178–1184.
13 S. M. Fenton, P. Padmanabhan, B. K. Ryu, T. T. Nguyen, R. N. Zia and M. E. Helgeson, Minimal conditions for solidification and thermal processing of colloidal gels, *Proc. Natl. Acad. Sci. U. S. A.*, 2023, **120**(25), e2215922120.
14 M. Das and G. Petekidis, Shear induced tuning and memory effects in colloidal gels of rods and spheres, *J. Chem. Phys.*, 2022, **157**(23), 234902.
15 S. Aime, L. Cipelletti and L. Ramos, Power law viscoelasticity of a fractal colloidal gel, *J. Rheol.*, 2018, **62**(6), 1429–1441.
16 W. C. Poon, The physics of a model colloid–polymer mixture, *J. Phys.: Condens. Matter*, 2002, **14**(33), R859.
17 S. M. Ilett, A. Orrock, W. Poon and P. Pusey, Phase behavior of a model colloid-polymer mixture, *Phys. Rev. E: Stat. Phys., Plasmas, Fluids, Relat. Interdiscip. Top.*, 1995, **51**(2), 1344.
18 S. Ramakrishnan, V. Gopalakrishnan and C. Zukoski, Clustering and mechanics in dense depletion and thermal gels, *Langmuir*, 2005, **21**(22), 9917–9925.
19 M. Dijkstra, R. van Roij and R. Evans, Phase diagram of highly asymmetric binary hard-sphere mixtures, *Phys. Rev. E: Stat. Phys., Plasmas, Fluids, Relat. Interdiscip. Top.*, 1999, **59**(5), 5744.
20 C. J. Dibble, M. Kogan and M. J. Solomon, Structure and dynamics of colloidal depletion gels: coincidence of transitions and heterogeneity, *Phys. Rev. E: Stat., Nonlinear, Soft Matter Phys.*, 2006, **74**(4), 041403.
21 R. N. Zia, B. J. Landrum and W. B. Russel, A micro-mechanical study of coarsening and rheology of colloidal gels: cage building, cage hopping, and Smoluchowski's ratchet, *J. Rheol.*, 2014, **58**(5), 1121–1157.
22 P. J. Lu, E. Zaccarelli, F. Ciulla, A. B. Schofield, F. Sciortino and D. A. Weitz, Gelation of particles with short-range attraction, *Nature*, 2008, **453**(7194), 499–503.
23 D. Mangal, G. S. Vera, S. Aime and S. Jamali, Small variations in particle-level interactions lead to large structural heterogeneities in colloidal gels, *Soft Matter*, 2024, **20**(24), 4692–4698.
24 P. J. Lu and D. A. Weitz, Colloidal particles: crystals, glasses, and gels, *Annu. Rev. Condens. Matter Phys.*, 2013, **4**(1), 217–233.
25 A. Boromand, S. Jamali and J. M. Maia, Structural fingerprints of yielding mechanisms in attractive colloidal gels, *Soft Matter*, 2017, **13**(2), 458–473.
26 J. Rouwhorst, C. Ness, S. Stoyanov, A. Zaccone and P. Schall, Nonequilibrium continuous phase transition in colloidal gelation with short-range attraction, *Nat. Commun.*, 2020, **11**(1), 3558.
27 W. H. Shih, W. Y. Shih, S. I. Kim, J. Liu and I. A. Aksay, Scaling behavior of the elastic properties of colloidal gels, *Phys. Rev. A: At., Mol., Opt. Phys.*, 1990, **42**(8), 4772.
28 M. Nabizadeh, F. Nasirian, X. Li, Y. Saraswat, R. Waheibi and L. C. Hsiao, *et al.*, Network physics of attractive colloidal gels: resilience, rigidity, and phase diagram, *Proc. Natl. Acad. Sci. U. S. A.*, 2024, **121**(3), e2316394121.
29 M. Kolb, R. Botet and R. Jullien, Scaling of kinetically growing clusters, *Phys. Rev. Lett.*, 1983, **51**(13), 1123.
30 P. Meakin, Formation of fractal clusters and networks by irreversible diffusion-limited aggregation, *Phys. Rev. Lett.*, 1983, **51**(13), 1119.
31 H. Tsurusawa, M. Leocmach, J. Russo and H. Tanaka, Direct link between mechanical stability in gels and percolation of isostatic particles, *Sci. Adv.*, 2019, **5**(5), eaav6090.
32 B. K. Ryu, S. M. Fenton, T. T. Nguyen, M. E. Helgeson and R. N. Zia, Modeling colloidal interactions that predict equilibrium and non-equilibrium states, *J. Chem. Phys.*, 2022, **156**(22), 224101.
33 E. Zaccarelli, Colloidal gels: equilibrium and non-equilibrium routes, *J. Phys.: Condens. Matter*, 2007, **19**(32), 323101.
34 A. P. Eberle, R. Castan eda-Priego, J. M. Kim and N. J. Wagner, Dynamical arrest, percolation, gelation, and glass formation in model nanoparticle dispersions with thermoreversible adhesive interactions, *Langmuir*, 2012, **28**(3), 1866–1878.
35 A. P. Eberle, N. J. Wagner and R. Castaneda-Priego, Dynamical arrest transition in nanoparticle dispersions with short-range interactions, *Phys. Rev. Lett.*, 2011, **106**(10), 105704.
36 Y. Chiew and E. Glandt, Percolation behaviour of permeable and of adhesive spheres, *J. Phys. A: Math. Gen.*, 1983, **16**(11), 2599.
37 A. Zaccone, D. Gentili, H. Wu, M. Morbidelli and E. Del Gado, Shear-driven solidification of dilute colloidal suspensions, *Phys. Rev. Lett.*, 2011, **106**(13), 138301.
38 K. A. Whitaker, Z. Varga, L. C. Hsiao, M. J. Solomon, J. W. Swan and E. M. Furst, Colloidal gel elasticity arises from the

 

packing of locally glassy clusters, *Nat. Commun.*, 2019, **10**(1), 2237.
39 J. H. Cho, R. Cerbino and I. Bischofberger, Emergence of multiscale dynamics in colloidal gels, *Phys. Rev. Lett.*, 2020, **124**(8), 088005.
40 M. E. Helgeson, Y. Gao, S. E. Moran, J. Lee, M. Godfrin and A. Tripathi, *et al.*, Homogeneous percolation versus arrested phase separation in attractively-driven nanoemulsion colloidal gels, *Soft Matter*, 2014, **10**(17), 3122–3133.
41 J. M. Van Doorn, J. Bronkhorst, R. Higler, T. Van De Laar and J. Sprakel, Linking particle dynamics to local connectivity in colloidal gels, *Phys. Rev. Lett.*, 2017, **118**(18), 188001.
42 P. Hoogerbrugge and J. Koelman, Simulating microscopic hydrodynamic phenomena with dissipative particle dynamics, *Europhys. Lett.*, 1992, **19**(3), 155.
43 P. Espanol and P. B. Warren, Perspective: dissipative particle dynamics, *J. Chem. Phys.*, 2017, **146**(15), 150901.
44 P. De Palma, P. Valentini and M. Napolitano, Dissipative particle dynamics simulation of a colloidal micropump, *Phys. Fluids*, 2006, **18**(2), 027103.
45 M. Nabizadeh and S. Jamali, Life and death of colloidal bonds control the rate-dependent rheology of gels, *Nat. Commun.*, 2021, **12**(1), 4274.
46 D. Mangal and S. Jamali, Role of interaction range on the microstructure and dynamics of attractive colloidal systems, *Soft Matter*, 2024, **20**(22), 4466–4473.
47 R. D. Groot and P. B. Warren, Dissipative particle dynamics: bridging the gap between atomistic and mesoscopic simulation, *J. Chem. Phys.*, 1997, **107**(11), 4423–4435.
48 P. D. Godfrin, N. E. Valadez-Pérez, R. Castaneda-Priego, N. J. Wagner and Y. Liu, Generalized phase behavior of cluster formation in colloidal dispersions with competing interactions, *Soft Matter*, 2014, **10**(28), 5061–5071.
49 E. Del Gado and W. Kob, Structure and relaxation dynamics of a colloidal gel, *Europhys. Lett.*, 2005, **72**(6), 1032.
50 Y. Li, J. R. Royer, J. Sun and C. Ness, Impact of granular inclusions on the phase behavior of colloidal gels, *Soft Matter*, 2023, **19**(7), 1342–1347.
51 K. Ioannidou, *et al.*, The crucial effect of early-stage gelation on the mechanical properties of cement hydrates, *Nat. Commun.*, 2016, **7**(1), 12106.
52 L. C. Hsiao, R. S. Newman, S. C. Glotzer and M. J. Solomon, Role of isostaticity and load-bearing microstructure in the elasticity of yielded colloidal gels, *Proc. Natl. Acad. Sci. U. S. A.*, 2012, **109**(40), 16029–16034.
53 A. Coniglio, L. De Arcangelis, E. Del Gado, A. Fierro and N. Sator, Percolation, gelation and dynamical behaviour in colloids, *J. Phys.: Condens. Matter*, 2004, **16**(42), S4831.
54 M. Gimperlein, J. N. Immink and M. Schmiedeberg, Dilute gel networks vs. clumpy gels in colloidal systems with a competition between repulsive and attractive interactions, *Soft Matter*, 2024, **20**(14), 3143–3153.
55 A. Aharony and D. Stauffer, *Introduction to percolation theory*, Taylor & Francis, 2003.
56 J. P. Singh, S. D. Walsh and D. L. Koch, Brownian dynamics of a suspension of particles with constrained voronoi cell volumes, *Langmuir*, 2015, **31**(24), 6829–6841.
57 K. S. Schweizer and E. J. Saltzman, Theory of dynamic barriers, activated hopping, and the glass transition in polymer melts, *J. Chem. Phys.*, 2004, **121**(4), 1984–2000.
58 H. Tanaka, Roles of liquid structural ordering in glass transition, crystallization, and water's anomalies, *J. Non-Cryst. Solids: X*, 2022, **13**, 100076.
59 S. Zhang, L. Zhang, M. Bouzid, D. Z. Rocklin, E. Del Gado and X. Mao, Correlated rigidity percolation and colloidal gels, *Phys. Rev. Lett.*, 2019, **123**(5), 058001.